2010 American Control Conference
Marriott Waterfront, Baltimore, MD, USA
June 30-July 02, 2010

Optimal Configuration Design for Hydraulic Split Hybrid Vehicles

Chiao-Ting Li and Huei Peng

Abstract—**Hydraulic hybrid vehicles are more suitable for heavy-duty applications in urban driving than hybrid electric vehicles because of the high power density and low cost of hydraulic devices. However, the low rotational speeds of hydraulic pump/motor and the low energy density of the accumulator impose severe constraints on the design and control for these vehicles. The split configuration is an efficient and more flexible transmission configuration and is the focus of this study. A three-step design methodology is developed to systematically and exhaustively explore all possible split configurations using two planetary gears: Step 1 checks mechanical feasibility of configurations; Step 2 develops optimal power management inspired by Pontryagin's Minimum Principle; and Step 3 finds optimal component sizes. After the screening, we identify three new configurations that achieve best fuel economy for the hydraulic vehicle/drive cycle studied, together with their best design and control executions.**

I. Introduction

RISING gasoline prices and environmental concerns are strong driving forces for high-efficiency vehicle technologies in recent years. Hybrid technologies have received great attention due to their proven effectiveness in reducing fuel consumption. Significant research has been done on hybrid electric vehicles (HEVs) for passenger cars, and about a dozen HEVs are now available in the US market. For heavy-duty applications, hybrid hydraulic vehicles (HHVs) are important alternatives because they are more cost effective and have much higher power density and reliability [1-4]. Hydraulic devices have very different dynamic characteristics from electric motors and batteries, and we cannot always adopt knowledge from HEV designs directly. To achieve optimal fuel economy in HHVs, configurations, power management and component sizes need to be tailored to match the new vehicle and component characteristics.

Hybrid vehicle configurations refer to the different ways of connecting the engine, motor, wheels, and clutches together through the split device. Some HHVs used series configurations [5] and parallel configurations [6-7], but they focus mostly on performance simulations after the configuration is selected. The split configuration can take advantages of both series and parallel configurations if the power management algorithm is properly designed [8-9]. Nevertheless, selecting a split configuration is complicated due to the large candidate pool—assuming patent ownership is not the only consideration. A systematic split hybrid configuration design methodology for HEVs was introduced [10]. In this paper, the design methodology pioneered in [10] is adopted and modified for the design of HHVs.

In addition to configuration, power management and components sizing are two important design elements that affects hybrid vehicle performance. Dynamic programming (DP) guarantees global optimality and has been used in HEV research [11]. Its main shortcoming is that it is very computationally intensive. In addition, the result cannot be implemented directly. The Pontryagin's minimum principle (PMP) is an alternative with much less computation requirement, but it only satisfies the necessary but not sufficient conditions for optimality [12-13]. Heuristic approaches sometimes also produce near-optimal results. For example, the Equivalent Consumption Minimization Strategy (ECMS) is an instantaneous optimization approach with a cost function similar to PMP [14], and can be implemented efficiently. The tradeoff between optimality and computational time is always a difficult design decision, and we decide that a near-optimal solution may be sufficient at the vehicle configuration design stage. In our research, since the design candidate pool is large, it is important to select a fast computation method.

The main goal of this paper is to present a comprehensive methodology and its application to the design of a hydraulic hybrid delivery truck, covering configuration screening, power management, and component sizing aspects of the design. The organization of this paper is as follows: in Section II, a HHV model is developed with a gear connection matrix specially arranged to represent all configuration candidates; Section III presents the three-step design methodology; Section IV presents results of the delivery truck design; and finally, conclusions are discussed in Section V.

II. Hydraulic Vehicle Modeling

In this paper, we design HHVs that use a split device with two planetary gears (PG). Hybrid vehicles with one PG (such as Toyota Prius) are popular but are limited in their operations. For heavier vehicles such as SUVs and larger passenger sedans, additional planetary gear was used to achieve the required torque/speed. Since we are designing a delivery truck, it is necessary to use two PGs, which can also better accommodate the low rotational speeds of hydraulic actuators. The HHV is assumes to have three power sources: an engine, a hydraulic pump and a hydraulic motor.

The core of the HHV model is a matrix describing the connection of the power devices and the vehicle. Models for the hydraulic components and the engine are built with

Manuscript received September 15, 2009.

Chiao-Ting Li is a Ph.D. student, and Huei Peng is a professor, both with the Department of Mechanical Engineering, University of Michigan (corresponding e-mail: hpeng@umich.edu).

system-level accuracy, and only longitudinal dynamics are considered.

A. Configuration Gear Connection Matrix

Before discussing details for the two-PG configuration, the single PG's dynamics are first reviewed. Figure 1 shows a PG and its equivalent lever diagram [15]. The speeds of the ring gear ω_r, sun gear ω_s, and carrier ω_c satisfy the following relationship:

$$\omega_s S + \omega_r R = \omega_c (R + S) \tag{1}$$

where S and R are the radii of the sun gear and ring gear.

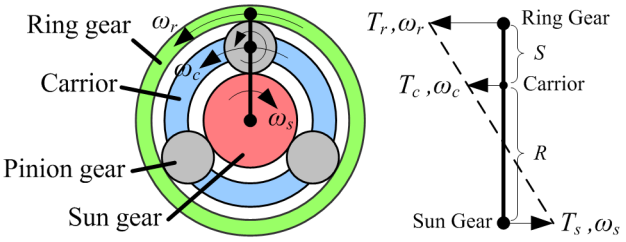

Figure 1. Planetary gearset and its lever diagram [16]

Figure 2 is an example two-PG split-hybrid configuration [10], shown in the lever diagram. The engine, hydraulic pump, and hydraulic motor are connected to the first PG (PG_1); the final drive (K) and wheels are connected to the second PG (PG_2). The lever lengths, S_1, R_1, S_2, and R_2, are gear radii. C_1 and C_2 are clutches. The configuration shifts between Mode 1 and Mode 2 by closing/opening the clutches. The two modes have different input-to-output gear ratios; the higher gear ratio is appropriate for launching and the lower gear ratio is suitable for high speed driving. In this paper, we perform an exhaustive search through, and all possible configurations with ring/sun gear ratios 1.5-2.5 are all searched.

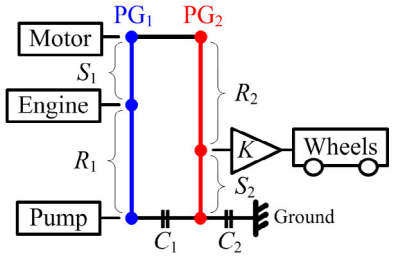

Figure 2. Lever diagram of a two-PG configuration

The speed relationship and torque relationship of this configuration with clutch C_1 open and C_2 closed (Mode 1) were written in the matrix form; the first four rows represent the engine, wheel, pump, and motor dynamics, and the last two rows are from the speed relationships on the two PGs [10]:

$$\begin{bmatrix} I_e & 0 & 0 & 0 & R_1+S_1 & 0 \\ 0 & \frac{Mr^2}{K^2} & 0 & 0 & 0 & R_2+S_2 \\ 0 & 0 & I_p & 0 & -S_1 & 0 \\ 0 & 0 & 0 & I_m & -R_1 & -S_2 \\ R_1+S_1 & 0 & -S_1 & -R_1 & 0 & 0 \\ 0 & R_2+S_2 & 0 & -S_2 & 0 & 0 \end{bmatrix} \begin{bmatrix} \dot{\omega}_e \\ \dot{\omega}_{out} \\ \dot{\omega}_p \\ \dot{\omega}_m \\ F_1 \\ F_2 \end{bmatrix} = \begin{bmatrix} T_e \\ T_{load} \\ T_p \\ T_m \\ 0 \\ 0 \end{bmatrix} \tag{2}$$

where ω_e, ω_p, ω_m, ω_{out} are the rotational speeds of the engine, pump, motor and PG_2 output; I_e, I_p, I_m, are inertias of the engine, pump and motor; and T_e, T_p, T_m are torques from the engine, pump and motor. T_{load} is the road load including air-resistance and rolling resistance. F_1 and F_2 are internal forces acting on the pinion gear teeth. M is the vehicle mass, and r is the tire radius. The first matrix on the left side of (2) is further divided into four sub-matrices:

$$\left[\begin{array}{cccc:cc} I_e & 0 & 0 & 0 & R_1+S_1 & 0 \\ 0 & \frac{Mr^2}{K^2} & 0 & 0 & 0 & R_2+S_2 \\ 0 & 0 & I_p & 0 & -S_1 & 0 \\ 0 & 0 & 0 & I_m & -R_1 & -S_2 \\ \hdashline R_1+S_1 & 0 & -S_1 & -R_1 & 0 & 0 \\ 0 & R_2+S_2 & 0 & -S_2 & 0 & 0 \end{array}\right] = \begin{bmatrix} I & D \\ D^T & 0 \end{bmatrix} \tag{3}$$

where I holds component inertias; D and D^T shows the gear connections. The 2-by-4 matrix D is called the *configuration gear connection matrix*, and by changing D, all possible two-PG split hybrid configurations can be represented. From the permutation there are 1,152 possibilities.

The component torque and speed relationships can be further derived by applying matrix algebra on D. Assuming the component inertias are negligible and with D_{EV} and D_{PM} defined as the upper half and lower half of the D matrix, the first four rows of (2) are rewritten as (4) and the last two rows are rewritten as (5).

$$\begin{bmatrix} T_p \\ T_m \end{bmatrix} = D_{PM} D_{EV}^{-1} \begin{bmatrix} T_e \\ T_{load} - \frac{Mr^2}{K^2}\dot{\omega}_{out} \end{bmatrix} \tag{4}$$

$$\begin{bmatrix} \omega_p \\ \omega_m \end{bmatrix} = -D_{PM}^{-T} D_{EV}^{T} \begin{bmatrix} \omega_e \\ \omega_{out} \end{bmatrix} \tag{5}$$

B. Hydraulic Pump/Motor

The hydraulic pump and motor are assumed to be variable-displacement type, and the torque $T_{p/m}$ and hydraulic fluid flow rate Q are assumed to be commanded by a displacement command x (with value between 0 and 1):

$$T_{p/m} = \begin{cases} \frac{1}{\eta_t} xL\Delta p, & \text{pumping} \\ \eta_t xL\Delta p, & \text{motoring} \end{cases} \tag{6}$$

$$Q = \begin{cases} \eta_v xL\omega_{p/m}, & \text{pumping} \\ \frac{1}{\eta_v} xL\omega_{p/m}, & \text{motoring} \end{cases} \tag{7}$$

where η_t and η_v are the torque and volumetric efficiencies, L is the pump/motor displacement per radian, and Δp is the pressure difference between the accumulator and reservoir.

A key issue of hydraulic devices is that they have a low maximum rotational speed (usually less than 4,000 rpm) than electric motors (12,000 rpm and higher). This characteristic will be further discussed in Section III.

C. Accumulator

The power storage device consists of an accumulator and an oil reservoir. The accumulator has a bladder inside to hold

Nitrogen gas. When the hydraulic fluid (oil) flows in, the gas is compressed and the internal energy increases. The state of charge (SOC) is defined as the normalized available volume in the accumulator. Assuming the hydraulic fluid is incompressible, the gas volume change is the same as the fluid flow rate, and the SOC dynamic is modeled as:

$$S\dot{O}C = \frac{\dot{V} - V_{\min}}{V_{\max} - V_{\min}} = \frac{Q - V_{\min}}{V_{\max} - V_{\min}} \tag{8}$$

where $\dot{V}$ is the gas volume change; $V_{\min}$ and $V_{\max}$ are the minimum and maximum gas volume in the accumulator. The pressure of the accumulator is described by the Benedict-Webb-Rubin equation [17]:

$$\begin{aligned} p = {} & \frac{RT}{v} + \left(B_0 RT - A_0 - C_0 / T^2\right) / v^2 \\ & + \left(bRT - a\right) / v^3 + a\alpha / v^6 + \left[C\left(1 + \gamma / v^2\right) e^{-\gamma / v^2}\right] / v^3 T^2 \end{aligned} \tag{9}$$

where R is the gas constant, T is the temperature, v is the specific volume of Nitrogen, A_0, B_0, C_0, a, b, α and γ are gas-dependent constants.

Frictional losses due to flow entrance effects and moving parts are assumed to result in a 2% pressure drop, and the hydraulic resistance loss is modeled to be proportional to the "equivalent pipe length" [18].

D. Engine

The engine model uses a BSFC look-up table to provide fuel consumption as a function of engine speed and torque. Transient responses, such as fuel injection, spark timing, and turbo-charge are ignored.

III. Design Methodology

The design methodology consists of three steps: Step 1 is the mechanical feasibility check, which quickly reduces the candidate pool by checking gear connection singularity and kinematic constraints; Step 2 optimizes the fuel consumption in simplified driving schedules to retrieve rules as the power management; and Step 3 finds the optimal values of key component parameters to determine the best configuration design.

A. Mechanical Feasibility

The mechanical feasibility checks whether the configuration results in proper input/output relationships, including non-singular gear connection, engine-to-wheel ratio, and feasibility of mode shifts [10]. These feasibility concepts for HHVs are identical to those of HEVs, even though the threshold values are different. In addition, for HHVs, ensuring low hydraulic motor/pump speed is an important constraint because hydraulic machines have much lower maximum rotational speeds than electric machines. From (5), the extreme pump/motor speeds may occur in one of the four situations: 1) both ω_e and ω_{out} are at maxima, 2) ω_e is at maximum and ω_{out} is at minimum, 3) ω_e is at minimum and ω_{out} is at maximum, or 4) both ω_e and ω_{out} are at minima. The above four conditions are examined in (5) to ensure that the hydraulic pump and motor speeds are below 4000 rpm.

B. Optimal Fuel Consumption

Configurations surviving the mechanical feasibility check proceed with fuel consumption optimization. The optimization problem is defined as follows:

$$\min\left\{J = \int L\left(T_e, \omega_e\right) dt\right\} \tag{10}$$

subject to

$$S\dot{O}C = f\left(SOC, T_e, \omega_e\right)$$

Component torque relationship (eq. 4)

Component speed relationship (eq. 5)

$$SOC_{\min} \le SOC \le SOC_{\max}$$

$$T_{\min} \le T_e \le T_{\max}$$

$$\omega_{\min} \le \omega_e \le \omega_{\max}$$

where $L(T_e, \omega_e)$ is the fuel consumption.

C. Inner –Loop Optimization [19]

Before solving the optimization problem shown in (10), an inner-loop optimization is conducted to reduce (10) to only one control variable, the net hydraulic power P_h. This can be done by writing P_h in terms of T_e and ω_e (using (5) and (4)). Then, the inner-loop optimization is defined as:

$$\begin{aligned} & \min L\left(T_e, \omega_e\right) \\ & \text{subject to} \\ & \quad P_h = h\left(T_e, \omega_e\right) \end{aligned} \tag{11}$$

The optima are found by collecting minimum fuel consumptions along each constant P_h curves (the dotted-line in Figure 3). The resulting P_h vs. $L(P_h)$ curve are shown in Figure 4, which can be interpreted as the minimum fuel needed to charge P_h into the accumulator. Note that the optimization reduction relies on the assumption that engine speed can rise as fast as needed; one might revise such an assumption by considering constraints on engine acceleration.

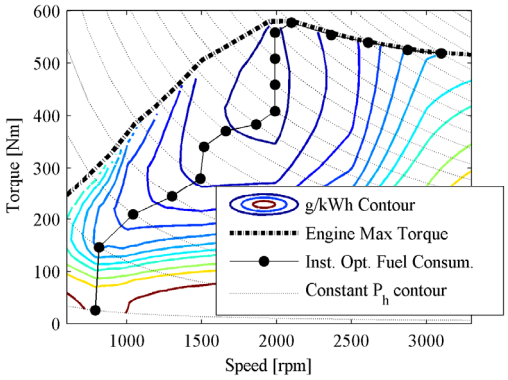

Figure 3. Inner-loop optimization at vehicle speed = 15 mph, torque = 690 Nm, and SOC = 98%

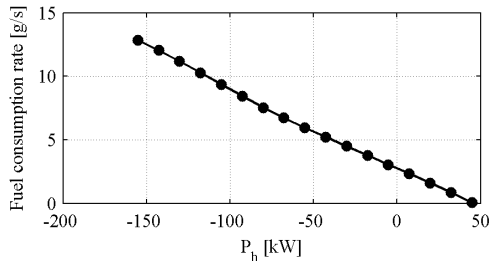

Figure 4. The optimal fuel consumption when vehicle speed = 15 mph, torque = 690 Nm, and SOC = 98%

Now, the optimization problem in (10) becomes:

$$\min\left\{J=\int L\left(P_h\right)dt\right\} \tag{12}$$

subject to

$$S\dot{O}C = f\left(SOC, P_h\right) \tag{13}$$

Component torque relationship (eq. 4) (14)

Component speed relationship (eq. 5) (15)

$$SOC_{\min} \le SOC \le SOC_{\max} \tag{16}$$

$$P_{\min} \le P_h \le P_{\max} \tag{17}$$

which is a constrained optimization problem with one state, *SOC*, and one control variable, P_h.

D. Pontryagin's Minimum Principle (PMP)

To solve (12) - (17) by PMP, define Hamiltonian:

$$H = L\left(P_h\right) + \lambda \cdot f\left(SOC, P_h\right) \tag{18}$$

where λ is the Lagrange multiplier. From PMP, the state and Lagrange multiplier must satisfy the following equations:

$$S\dot{O}C = \frac{\partial H}{\partial \lambda} = f\left(SOC, P_h\right) \tag{19}$$

$$\dot{\lambda} = -\frac{\partial H}{\partial\left(SOC\right)} = -\lambda\frac{\partial f}{\partial\left(SOC\right)} \tag{20}$$

The necessary condition for constrained optimality is [20]:

$$H\left(P_h^*, SOC^*, \lambda^*, t\right) \le H\left(P_h, SOC^*, \lambda^*, t\right) \tag{21}$$

with boundary conditions:

$$SOC\left(t_0\right) = SOC_0 \tag{22}$$

$$\lambda\left(t_f\right) = 1 \tag{23}$$

Equation (23) comes from the free terminal condition of SOC [21]. Equation (23) and (24) pose a two-point boundary value problem (TPBVP), which is non-trivial to solve. Instead of solving the TPBVP, a sub-optimal solution is evaluated, inspired by attempts to solve the Hamiltonian and observed hydraulic device characteristics. A unique characteristic of HHVs is that the accumulator has a very small capacity compared with a battery; however, heavy-duty vehicles have significant regenerative braking energy when decelerating due to their heavier weights. This means that the accumulator has to discharge quickly during launching to leave adequate room for regenerative braking energies. Another special characteristic of HHVs is that, unlike batteries, deep discharge is acceptable. Also, the inner-loop optimization indicates the fuel consumption is monotonically decreasing in P_h (see Figure 4), so it is expected that the solution is bounded by (16) or (17). By combining these characteristics of HHVs, a solution policy is constructed as:

$$\begin{aligned} &\text{If } SOC \ge SOC_{\min}, \\ &\quad P_h = \min\left\{P_{\max}, T_{load}\omega_{out}\right\} \quad , P_e = T_{load}\omega_{out} - P_h \\ &\text{Else} \\ &\quad \text{choose } P_h \text{ such that } S\dot{O}C = 0, P_e = T_{load}\omega_{out} + P_h \end{aligned} \tag{24}$$

where P_{max} is the maximum power of hydraulic devices, and P_e is the engine power. The P_h in the "Else" statement is not zero because of power circulation losses [22].

The solution policy (24) is *myopic* because it uses hydraulic power quickly without considering possible over-discharge in the future. This is similar to the concept of ECMS, with HEV battery expenditure being lightly penalized [14]. The near-optimality of (24) is validated in three simplified driving schedules. These simplified driving schedules, as shown in Figure 5, are chosen to represent typical driving patterns in FUDS: #1 resembles an aggressive launching and ensures drivability; #2 consists of five mild launchings, resembling the frequent stop-and-go at medium speed; and #3 resembles a cruising section.

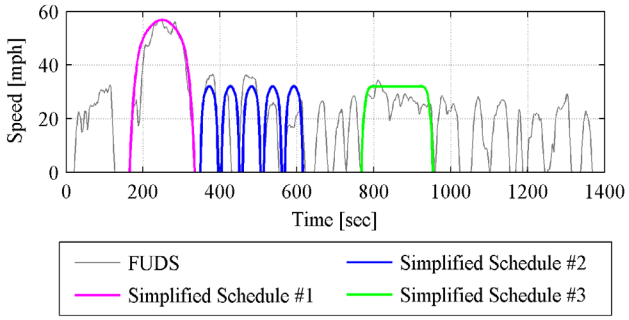

Figure 5. Speed profiles of FUDS and the simplified driving cycles

Simulations show that (24) are indeed near-optimal in all the three simplified driving schedules. The control behavior is very similar to the global optimum solution from DP. Figure 6 shows the myopic policy (24) and DP executions on Schedule #2, and the control actions are indistinguishable. Similar results were also found for Schedules #1 and #3. As a result, (24) will be used as the power management strategy in the design methodology to speed up the computation.

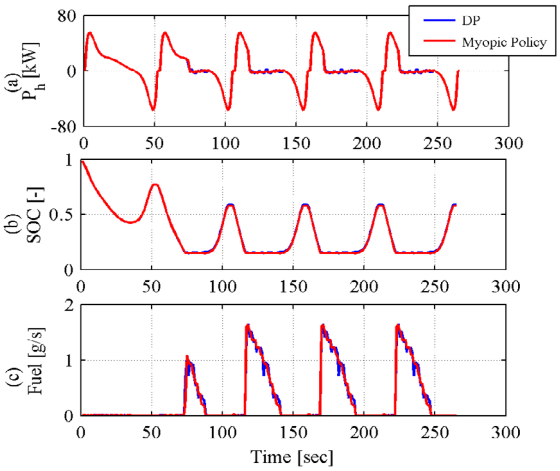

Figure 6. The comparison between the myopic policy (24) and DP results in the Simplified Driving Schedule #2

E. Component Sizing

Two component design parameters are explored: sizes of the PGs and the capacity of the accumulator. The main PG size parameter is the ratio between ring gear radius over the sun gear radius, and the accumulator capacity determines available hydraulic power, energy, size and cost.

PG ratios affect matrix D, so, while exploring different PG ratios, the speed constraint for mechanical feasibility needs to be re-examined, and so does drivability over Schedule #1.

The accumulator capacity affects the hydraulic output power and regenerative braking energy capture. The former is one of the factors that affect the drivability and the later relates to the fuel economy. Large gas tanks are preferred; however, they take more space and are heavier. By exploring the accumulator capacity, we can see the trade-off between the weight and vehicle performances.

The engine or hydraulic pump/motor torque scaling are excluded from our component sizing study. The reasons are as follows. First, HHVs have little room for engine downsizing because of the low energy content in the hydraulic accumulator. Accumulator depletion is expected to happen occasionally and the engine will have to propel the vehicle along. Second, upsizing the pump/motor is not necessary for the current vehicle specifications, since it only increases weight while the current devices already provide decent drivability. Downsizing has been attempted but failed in the drivability check.

Figure 7 summarizes the design methodology. All possible PG ratios were tested iteratively. Using the simplified near-optimal power management strategy, the computation is fast and the design iterations are solved within reasonable time. The computational time on each design is about 6 seconds in Schedule #1 and about 1 minute in FUDS on a 1.8 GHz duel core, 2GB RAM computer.

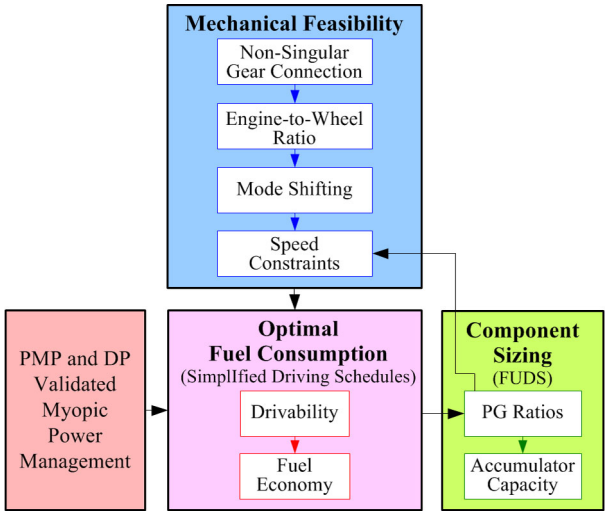

Figure 7. Flow chart of the design methodology

IV. Results

The proposed three-step design methodology is used to design a hydraulic split hybrid delivery truck as a case study. The target vehicle has a mass of 4,926 kg, 462 kg of which is the hydraulic components. The primary power source is a V6 4.5L diesel engine with a rated power of 127 kW at 2,100 rpm. The hydraulic pump and motor both have maximum displacement of 180cm^3/rev and the power range is 0-175 kW. The accumulator has volume as 110L and the maximum pressure is 40 MPa.

The design starts with a pool of 1,152 candidate configurations, and both PG ratios are initialized to start at 2. The number of valid configurations drops to 20 after the mechanical feasibility check, mainly due to the stringent actuator speed constraint. Fuel consumption optimization shows that seven configurations passed the drivability check; their normalized fuel economy is shown in Figure 8. Six configurations are more fuel efficient than the non-hybrid version of the truck, while three of them have significant improvements and their configurations are shown in Figure 9 (the lever lengths are not shown to scale).

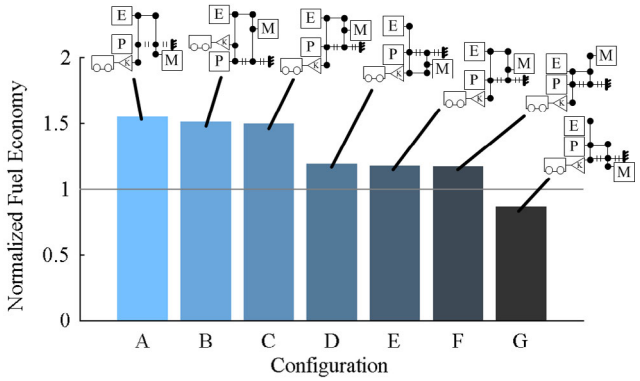

Figure 8. Fuel economy of the seven configurations that survive drivability check.

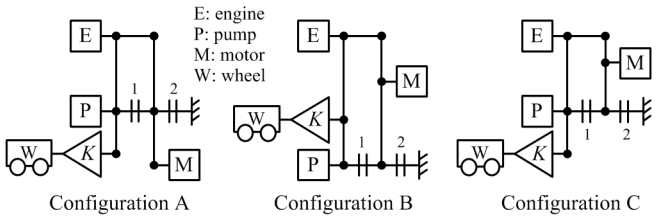

Figure 9. The top three configurations

The PG ratios between 1.5 and 2.5 are explored in component sizing to further improve the fuel economy.

The second component sizing parameter is accumulator capacity. The trade-off is that, for every 10% increase in the capacity, 23 kg will be added in weight. The optimized component sizes and fuel consumption of the top three configurations are listed in TABLE I.

TABLE I
COMPONENT SIZING RESULTS OF THE TOP THREE CONFIGURATIONS

Configuration	Non-Hybrid	A	B	C
PG Ratios	4 Speed transmission	$PG_1 = 2.25$, $PG_2 = 1.5$	$PG_1 = 2$ $PG_2 = 2$	$PG_1 = 2.5$ $PG_2 = 2.5$
Accumulator Capacity	N/A	110L	10% larger	10% larger
Vehicle Weight [kg]	4463	4926	4949	4949
Fuel use in FUDS [g]	1002	647	660	692

The best design is concluded to be Configuration A, which has the engine, pump, and final drive connected to the sun gear, carrier, and ring gear of PG_1, and the motor connected to the ring gear of PG_2. The optimized PG ratios are 2.25 for the first PG and 1.5 for the second PG, and the accumulator capacity happens to be the same as the baseline case. Its fuel economy is 54% better than the non-hybrid reference simulation.

V. CONCLUSION

This paper presents a methodology for the optimal design of hydraulic split hybrid vehicles. It has three steps: mechanical feasibility check, fuel consumption optimization, and component sizing optimization. In the mechanical feasibility check, we check for powertrain singularity and gear ratios, followed by a newly developed speed constraint check to accommodate the low rotational speed of hydraulic devices. To speed up computation, we adopt a myopic power management algorithm; the optimality is validated by comparing with DP results on three simplified driving schedules. The component sizing focuses on PG ratios and the accumulator capacity.

In the design process, two major HHV characteristics, the low hydraulic device speed and the small accumulator capacity, are addressed in the mechanical feasibility check and the myopic power management respectively. These characteristics also affect which component parameters we chose to explore in component sizing. As a result, the best three resulting configurations are different than existing split hybrid configurations used on HEVs.

In conclusion, the gear connection matrix fully exploits the design freedom of two-PG configuration, yet the design methodology are comprehensive and fast enough that we can explore the complete candidate pool exhaustively rather than only targeting a handful of configurations. The thorough exploration ensures no configuration went unexplored and the best designs were evaluated.

ACKNOWLEDGMENT

The authors would like to acknowledge Bosch-Rexroth for supporting this research. We also thank Prof. Zoran Filipi, and students in his group (Rajit Johri and Fernando Tavares) for insightful discussions.

REFERENCES

[1] L. O. Hewko and T. R. Weber, "Hydraulic Energy Storage Based Hybrid Propulsion System For A Terrestrial Vehicle," in *Proceedings of the 25th Intersociety Energy Conversion Engineering Conference*, 1990, pp. 99-105.

[2] P. Jirawattana*, et al.*, "Design of a Hydraulic Wheel Pump/Motor for a Hydrostatic Automobile," *SAE Paper,* 2002-01-1349.

[3] P. Matheson and J. Stecki, "Development and Simulation of a Hydraulic-Hybrid Powertrain for use in Commercial Heavy Vehicles," *SAE Paper,* 2003-01-3370.

[4] S. Baseley*, et al.*, "Hydraulic Hybrid Systems for Commercial Vehicles," *SAE Paper,* 2007-01-1455.

[5] Y. J. Kim and Z. Filipi, "Simulation Study of a Series Hydraulic Hybrid Propulsion System for a Light Truck," *SAE Paper,* 2007-01-4151.

[6] B. Wu*, et al.*, "Optimal Power Management for a Hydraulic Hybrid Delivery Truck," *Vehicle System Dynamics,* vol. 42, pp. 23-40, 2004.

[7] Z. Filip*, et al.*, "Combined optimisation of design and power management of the hydraulic hybrid propulsion system for the 6 × 6 medium truck," *Int. J. Heavy Vehicle Systems,* vol. 11, pp. 371-401, 2004.

[8] B. Conlon, "Comparative Analysis of Single and Combined Hybrid Electrically Variable Transmission Operating Modes," *SAE Paper,* 2005-01-1162.

[9] T. M. Grewe*, et al.*, "Defining the General Motors 2-Mode Hybrid Transmission," *SAE Paper,* 2007-01-0273.

[10] J. Liu, "Modeling, Configuration and Control Optimization of Power-Split Hybrid Vehicles," Ph.D. dissertation, Department of Mechanical Engineering, University of Michigan, Ann Arbor, 2007.

[11] C.-C. Lin*, et al.*, "Power Management Strategy for a Parallel Hybrid Electric Truck," *IEEE Transactions on Control Systems Technology,* vol. 11, pp. 839-849, 2003.

[12] S. Delprat*, et al.*, "Control Strategies for Hybrid Vehicles: Optimal Control," in *Vehicular Technology Conference*, Vancouver, Canada, 2002, pp. 24-28.

[13] G. Rousseau*, et al.*, "Constrained Optimization of Energy Management for a Mild-Hybrid Vehicle," in *Oil & Gas Science and Technology*, 2007, pp. 623-634.

[14] A. Sciarretta*, et al.*, "Optimal Control of Parallel Hybrid Electric Vehicles," *IEEE Trans. Veh. Technol,* vol. 12, pp. 352-363, 2004.

[15] H. Benford and M. Leising, "The Lever Analogy: A Now Tool in Transmission Analysis," *SAE Paper,* 1981.

[16] J. Liu and H. Peng, "Modeling and Control of a Power-Split Hybrid Vehicle," *IEEE Transactions on Control Systems Technology,* vol. 16, pp. 1242-1251, 2008.

[17] H. W. Cooper and J. C. Goldfrank, "B-W-R Consstants and New Correlations," *Hydrocarbon Processing,* vol. 46, pp. 141-146, 1967.

[18] A. Pourmovahed*, et al.*, "Modeling of a Hydraulic Energy Regeneration System-Part I: Analytical Treatment," *Journal of Dynamic Systems, Measurement, and Control,* vol. 114, pp. 155-159, 1992.

[19] N. Kim, "Energy Management Strategy For Hybrid Electric Vehicles Based On Pontryagin's Minimum Principle," Ph.D. dissertation, Department of Mechanical Engineering, Seoul National University, Seoul, 2009.

[20] D. E. Kirk, *Optimal Control Theory: An Indroduction*. New Jersy: Prentice-Hall, 1970.

[21] A. Bryson and Y.-C. Ho, *Applied Optimal Control*. New York: Hemisphere Publishing Coorporation, 1975.

[22] J. Miller, "Hybrid Electric Vehicle Propulsion System Architectures of the e-CVT Type," *IEEE Transactions on Power Electronics,* vol. 21, pp. 756-767, 2006.